vehicles

Article

Predictive Model of Adaptive Cruise Control Speed to Enhance Engine Operating Conditions

Srikanth Kolachalama * and Hafiz Malik

Electrical and Computer Engineering, University of Michigan, Dearborn, MI 48128, USA; hafiz@umich.edu
* Correspondence: skola@umich.edu

Abstract: This article presents a novel methodology to predict the optimal adaptive cruise control set speed profile (ACCSSP) by optimizing the engine operating conditions (EOC) considering vehicle level vectors (VLV) (body parameter, environment, driver behaviour) as the affecting parameters. This paper investigates engine operating conditions (EOC) criteria to develop a predictive model of ACCSSP in real-time. We developed a deep learning (DL) model using the NARX method to predict engine operating point (EOP) mapping the VLV. We used real-world field data obtained from Cadillac test vehicles driven by activating the ACC feature for developing the DL model. We used a realistic set of assumptions to estimate the VLV for the future time steps for the range of allowable speed values and applied them at the input of the developed DL model to generate multiple sets of EOP's. We imposed the defined EOC criteria on these EOPs, and the top three modes of speeds satisfying all the requirements are derived at each second. Thus, three eligible speed values are estimated for each second, and an additional criterion is defined to generate a unique ACCSSP for future time steps. A performance comparison between predicted and constant ACCSSP's indicates that the predictive model outperforms constant ACCSSP.

Keywords: adaptive cruise control; driver behaviour; deep learning; engine operating point

Citation: Kolachalama, S.; Malik, H. Predictive Model of Adaptive Cruise Control Speed to Enhance Engine Operating Conditions. *Vehicles* **2021**, *3*, 749–763. https://doi.org/10.3390/vehicles3040044

Academic Editor: Pak Kin Wong

Received: 16 October 2021
Accepted: 4 November 2021
Published: 9 November 2021

1. Introduction

The introduction of automobiles into the world inculcated innovation in many aspects of engineering, including design and manufacturing (Townsend and Calantone, 2014) [1]. Engineers worldwide continuously strive to develop cutting-edge technologies to augment the riders' comfort, traffic behaviour, enhance safety and fuel economy (Katzenbach, 2015) [2]. In the current scenario, advanced features which include forward collision, traction control, and lane change, augment the safety, whereas the fuel economy drive mode reduces the fuel consumption. Among the features integrated into the vehicle, the ACC system developed by Labuhn and Chundrlik, 1995 played a vital dual role, in affecting safety and EOC [3]. The intricate concept of the ACC system is to produce controlled acceleration without disengaging the cruise in the user-defined proximity and strictly follow the user command of set speed (Marsden et al., 2001) [4]. Additionally, we could conclude from the existing literature (Mahdinia et al., 2020) that the activation of ACC results in lower IFCR [5]. Therefore, activating the ACC feature for traversing long trips would augment EOC.

However, identifying the optimal ACCSSP by considering the dynamic state of the vehicle for a definite coordinate on the terrain is an unsolved, challenging task for engineers. Researchers have performed the parametric optimisation of ACC output in the existing literature by analysing the real-time data of behaviour, traffic congestion, terrain data, and environmental factors. Stanton et al., 2005, Hoedemaeker et al., 1998, Kesting et al., 2007, Rudin-Brown et al., 2004, Moon et al., 2008, and Rosenfeld et al., 2015 considered driver behaviour as the key input to develop the control algorithm using analytical techniques and to tune the outputs of the ACC system [6–11]. The enhancements of vehicle connectivity opened doors to obtain real-time traffic congestion information. Milanés et al., 2013:2014, Kesting et al., 2008:2007, and Ploeg et al., 2011, adopted the DL models to estimate the ACCSSP and desired acceleration based on the traffic congestion data retrieved in real-time [12–15]. Li et al., 2017, Lu et al., 2019, Vedam, 2015, Kolmanovsky and Filev, 2010, Gáspár and Németh, 2014:2011:2013, and Ma et al., 2019, adopted the terrain data to estimate the ACC control parameters to reduce IFCR using the known mathematical models [16–23].

Existing techniques rely on either one or two affecting factors as inputs to predict ACCSSP considered, but none of the researchers included all the factors in conjunction to the best of our knowledge. Recently, we developed a DL model mapping all the VLV and EOP (Kolachalama et al., 2021) [24]. This DL model produced the best results for the ACC activated test case and included all the factors mentioned above, excluding traffic congestion information. This paper applied predefined EOC criteria to the predicted EOP, and the optimal ACCSSP is estimated corresponding to augmented EOC. We validated the proposed model using the real-time test vehicle data-driven road segments that included arterial, state ways, and freeways. The below sections show the detailed procedure adopted.

The rest of the article is organised as follows: Sections 2 and 4 propose predicting EOP and ACCSSP, whereas Section 3 defines the EOC criteria applied to the EOP to estimate ACCSSP. In Section 5, the detailed results of the predictive model and experimental techniques are presented.

2. Predictive Model for EOP

We adopted the commonly available DL methods, NARX and LSTM, to develop predictive models involving time-sensitive data (Diaconescu, 2008) [25]. Kolachalama et al., 2021, compared NARX and LSTM methods using the real-time test case (2019 Cadillac XT6) and proved that the NARX method outperforms the LSTM model [24]. Hence, in this research, a similar NARX DL model is used with default training options to predict EOP, as shown in Table 1.

Table 1. Prediction of EOP—NARX DL model.

NARX—Deep Learning Model					
Properties		**Dataset—Training and Testing**			
Property	**Value**	**Vehicle**	**Training**	**Test Size**	**ACCSSP (MPH)**
Training function	Levenberg–Marquardt backpropagation	2020 Cadillac CT5	1–14,000	14,001–15,000	30
Input/Feedback delays	1:2	2020 Cadillac CT5	1–24,000	24,001–25,000	40
Training, Validation	[30,70]%	2020 Cadillac CT5	1–34,000	34,001–35,000	50
Hidden layer size	10	2020 Cadillac CT5	1–44,000	44,001–45,000	60
Network	Open	2019 Cadillac XT6	1–40,000	40,001–41,000	70
Performance	MSE	2021 Cadillac CT4	1–25,000	25,001–26,000	80

As mentioned in the previous section, Figure 1 depicts the DL model to predict the EOP mapping VLV. The outputs of the DL model consist of the elements IET, IES, and IFCR, and the VLV, which embed with driver behaviour, body module parameters, environmental factors, and terrain data. The DBV consists of three elements speeding (Speed, LOT), steering (YAR, LAT) and CAT (Kolachalama et al., 2021) [24,26]. The parameters odometer, tire pressure, curvature, and gradient affect the vehicle traction, whereas CAT and EAT influence thermal stress on the engine (Kolachalama et al., 2008) [27]. Additionally, there is no loss of generality in replacing the gradient with the vehicle posture's Euler angles, which affect the traction under no-slip (Eathakota et al., 2010) [28,29].

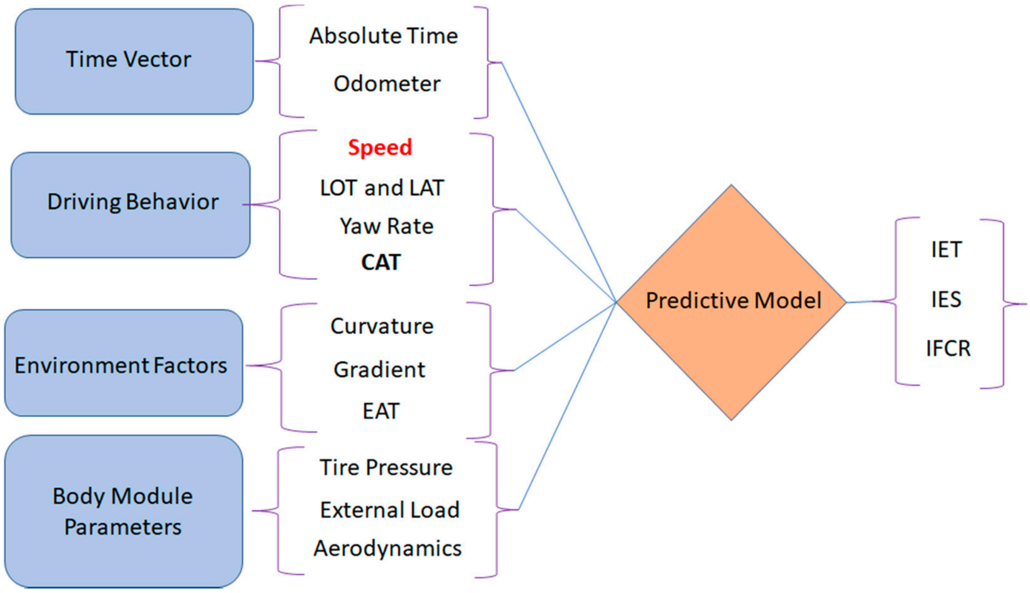

Figure 1. Predictive model—inputs and outputs [5].

3. Metric for Optimal EOC

In this section, we defined the metrics for EOC criteria, which reflect optimal EOP.

3.1. Generic Criteria

The predicted EOP for the vehicles traversing the speeds ranging [25 45] MPH (arterial roads) have a closer proximity to the ideal EOP. In this scenario, the IET has a higher magnitude; on the contrary, for the speeds ranging [65 85], MPH (freeways) have higher IES recorded.

Additionally, the allowable speeds for the state ways range between [45 65] MPH are considered the green zone with maximum fuel economy (low IFCR). Hence, the generic criteria for augmented EOC would include higher IET, higher IES, and lower IFCR, along with the maximum distance traversed for the trip.

3.2. Euclidean Distance—Ideal EOP

An engine map calibrated at the manufacturing plant for every model by all automotive OEM's represents the engine's performance. In general, the ideal EOP for any vehicle represents the coordinate (centroid) on the map with the lowest IFCR. An example of the engine map for the vehicle 2014 Chevrolet 4.3L EcoTec3 LV3 Engine is shown in Figure 2A. The ideal EOP for this vehicle was estimated to be the coordinate [285 Nm, 2250 RPM, 225 g/kwh]. Similarly, the ideal EOPs for the three test vehicles are empirically estimated, as shown in section A: Table 2.

Hence, we defined the line segment conjoining the predicted and ideal EOP as the EOC vector, represented by the IEM shown in Figure 2B. The magnitude of the EOC vector represents the ED_i shown in Equation (1). In the 2D plane, there is no loss of generality in ignoring the parameter IES, as it is proportional to the vehicle speed. Therefore, lower ED represents increased EOC.

$$ED_i = \sqrt{(IET_i - IET_k)^2 + (IFCR_i - IFCR_k)^2} \quad (1)$$

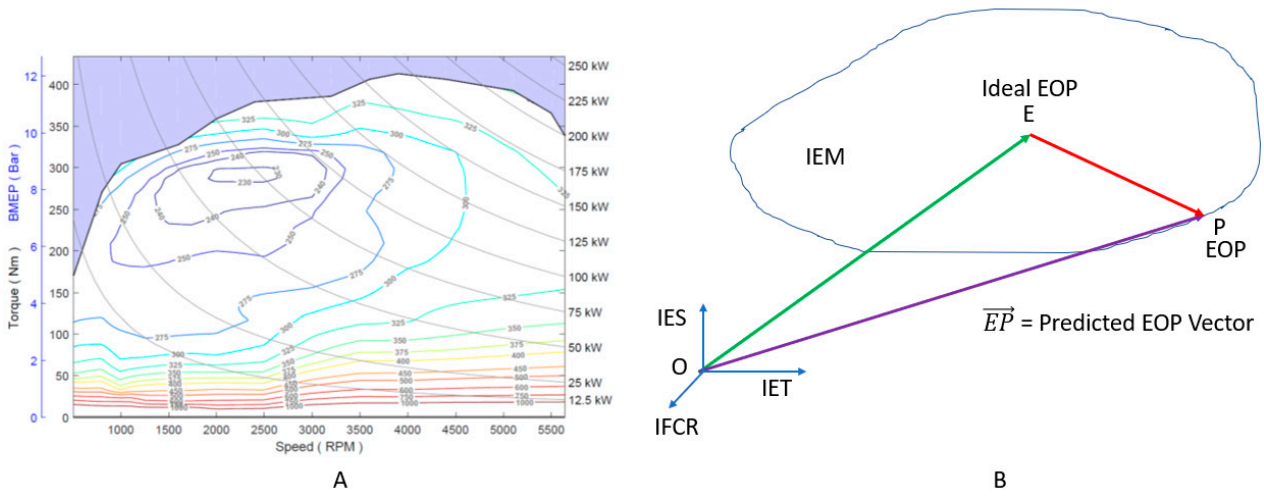

Figure 2. (**A**) Engine map: 2014 Chevrolet 4.3L; (**B**) IEM—EOC vector. Environmental Protection Agency, National Vehicle and Fuel Emissions Laboratory, National Center for Advanced Technology, Ann Arbor, Michigan, USA. Version 2018-08.

Table 2. EOC criteria—EOP.

Section A				Section B					
Ideal EOP				Generic		Engine Specific		Smoothness Measure—Spline Fit	
Vehicle	**IET (Nm)**	**IES (rad/s)**	**IFCR** $(1 \times 10^{-8}\ \mathbf{m^3 s^{-1}})$	**Parameter**	**Condition**	**Parameter**	**Condition**	**Parameter**	**Condition**
Cadillac CT5	250	140	180	IET	Higher	ED	Lower	R^2/Adj R^2	Higher
Cadillac XT6	280	145	220	IES	Higher	ESC	Higher	RMSE	Lower
Cadillac CT4	240	140	200	IFCR	Lower	ETC	Higher	SSE	Lower

3.3. Engine Caliber—Speed and Torque

The engine's capability is measured by two standard parameters [ESC, ETC]. These parameters are the ratios that define the torque produced per unit of fuel consumption and the speed produced per unit of torque. Higher ETC and ESC are the desired criteria for every vehicle's trip.

$$\mathrm{ETC} = \frac{IET}{IFCR} \tag{2}$$

$$\mathrm{ESC} = \frac{IES}{IET} \tag{3}$$

3.4. Smoothness Measure—EOC Parameters

The combustion of fuel in the engine produces torque with fluctuating magnitudes. However, all the elements of EOP should have smooth behaviour (Tanaka et al., 1987, Li et al., 2017) [30,31]. Hence, as an additional optimal EOC metric, we defined the smoothness measure for all the six parameters—IET, IES, IFCR, ED, ETC, ESC. We used the spline to fit the data points of EOC parameters by normalising the data. The optimal fit criteria were measured by traditional statistical techniques R^2/Adjusted R^2, RMSE, and SSE, using the built-in toolboxes of MATLAB as shown in section B: Table 2.

4. Prediction of ACCSSP

The prediction of ACCSSP was categorised into four steps, as described in the following sections.

4.1. Estimation of Future Input States—DL Model

Step 1: Relative to the current state of the vehicle (VLV_k), the future input values (VLV_{k+1}) of the DL model (Figure 3) are estimated using the relations shown in Table 3. The parameter odometer (O_{k+1}) was calculated using the speed (S_k) with the constant time step by basic linear interpolation. The LOT ($L_{o(k+1)}$) is estimated based on the vehicle resistance shown in the equation set in Table 3, and the parameters YAR ($Y_{a(k+1)}$) and LAT ($L_{a(k+1)}$) are calculated assuming ISB (Kolachalama et al., 2018) [25]. The environmental parameters EAT_{k+1}, terrain data, [RRC_{k+1}, $\theta_{g(k)}$], are retrieved using the GPS location and the infotainment maps. The magnitudes of the tire pressure (TP_{k+1}) and CAT_{k+1} are assumed to be equal to the previous time step (Table 4).

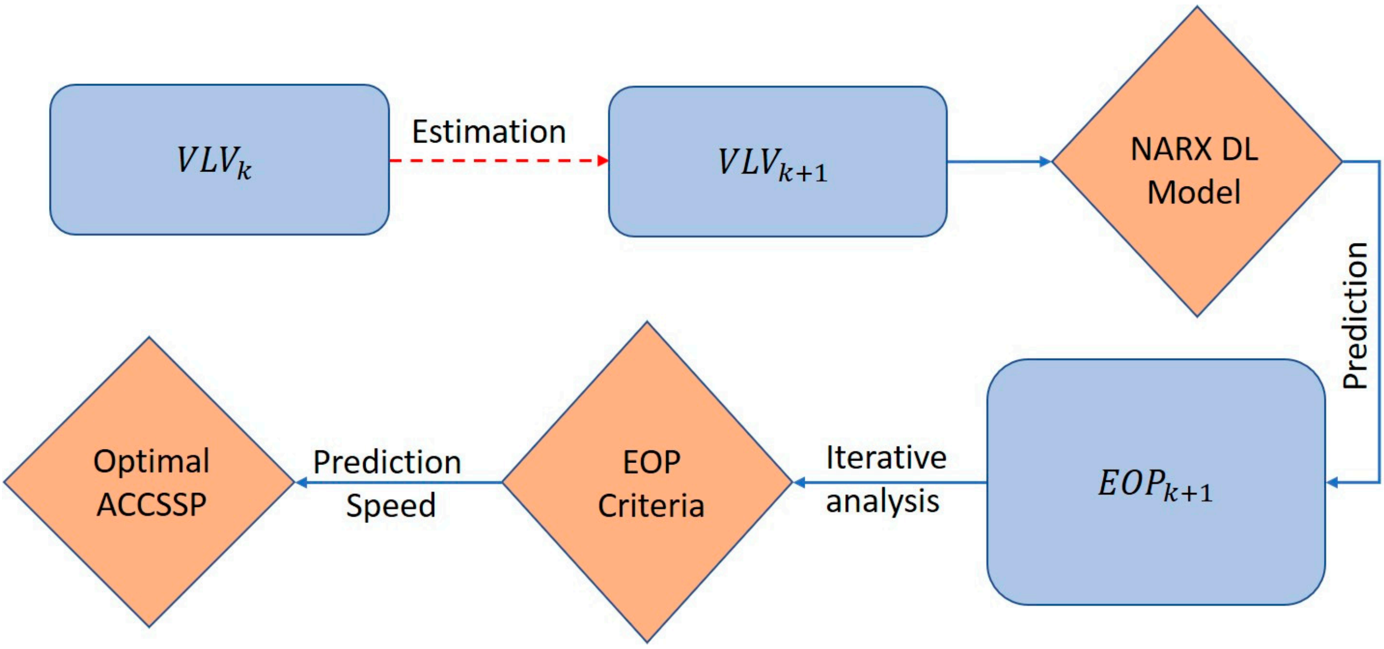

Figure 3. Process—Prediction of optimal ACCSSP.

Table 3. Equation set—prediction of future input states.

$RRC_{k+1},\ \theta_{g(k+1)}$	$2RRC_{k+1} = \frac{S_{k+1}^2}{L_{a(k+1)}} + \frac{S_{k+1}}{Y_{a(k+1)}},\ min\left[abs\left(Y_{a(k+1)}.S_{k+1} - L_{a(k+1)}\right)\right]$	$\rho = 1.225\ \text{kg·m}^{-3}$
$T_{k+1} = T_k + dT$	$L_{o(k+1)} = g\mu_r + g sin(\theta_{g(k+1)}) + \frac{\rho C_d.A_c}{2.(M_c+M_L)}.S_{k+1}^2$	$S_{k+1} = [SL - 10,\ SL]$
$O_{k+1} = O_k + S_k.dT$	2020 Cadillac CT5 : $M_c = 1769.69$ kg, $M_L = 76.8$ kg, $C_d = 0.31$, A = 1.71 m^2	$CAT_{k+1} = CAT_k$
$EAT_{k+1} = EAT_k$	2019 Cadillac XT6 : $M_c = 2050.278$ kg, $M_L = 76.8$ kg, $C_d = 0.35$, A = 1.88 m^2	g = 9.81 m·s^{-2}
$TP_{k+1} = TP_k$	2021 Cadillac CT4 : $M_c = 1626.94$ kg, $M_L = 76.8$ kg, $C_d = 0.30$, A = 1.70 m^2	$\mu_r = 0.013$

4.2. Prediction of Outputs—DL Model

Step 2: We estimated the input sets for future time steps (1 s—[T_0 T_1]) for the AVS range (e.g., [SL-10, SL]). Thus, we generated eleven sets of inputs, and fed them into the DL model, and predicted a corresponding eleven sets of outputs (EOP's) (Table 5).

Table 4. Predicted inputs—DL model, 2019 Cadillac XT6 (100 time steps = 1 s).

Time Step	Odometer (Miles)	Speed (MPH)	RRC (m)	YAR (deg/s)	LAT (m·s^{-2})	LOT (m·s^{-2})
T_0	15,000	70	8304.140	0.216	0.117	0.437
dT_{10}	15,000.001	70	8304.140	0.216	0.117	0.375
dT_{20}	15,000.003	70	8304.140	0.216	0.117	0.312
dT_{30}	15,000.005	70	9342.157	0.192	0.104	−0.125
dT_{40}	15,000.007	70	24,912.42	0.072	0.039	−0.187
dT_{50}	15,000.009	70	74,737.261	0.024	0.013	−0.062
dT_{60}	15,000.011	70	74,737.261	0.024	0.013	0.25
dT_{70}	15,000.013	70	37,368.630	0.048	0.026	0.25
dT_{80}	15,000.015	70	24,912.420	0.072	0.039	0.187
dT_{90}	15,000.017	70	24,912.420	0.072	0.039	0.187
T_1	15,000.019	70	9342.157	0.192	0.104	0.312

4.3. Estimation of ACC Speed Values—EOC Criteria

Step 3: We applied the EOC criteria defined in section III for the eleven predicted EOP's (Table 5). The top six performing speed values are selected for each EOC parameter, and hence, the top three modes of speeds (EVS) are calculated for each time step (Table 6). We incorporated a similar procedure for the next ten seconds, and the ACC Matrix (3X10) was developed (Table 7).

4.4. Algorithm to Predict ACCSSP

Step 4: Every second has three EVS, resulting in a maximum of 3^{10} possible ACCSSP's for 10 s. The following conditions are defined to identify a unique ACCSSP inspired by the Dubin path traverse problem (La Valle, 2011) [32].

1. Assuming the ACCSSP at T_k is S_k, if the EVS is either S_k+1, S_k, or S_k−1, the highest magnitude among the three is selected as S_{k+1};
2. S_1 is chosen closer to S_0 (IAS). If this results in two values, then the higher value is considered as S_1;
3. If the eligible speeds at T_{k+1} are neither $S_k + 1$, S_k, nor $S_k - 1$, then $S_{k+1} = S_k$;
4. If $S_{k+1} = S_k$ for more than 10 s, S_{k+1}= S_k + 1 if $S_k + 1 \leq$ SL or $S_k - 1$ if S_k = SL.

Table 5. EOC criteria—iteration of ACC Speeds (100 time steps).

EOP	Speed	65	66	67	68	69	70	71	72	73	74	75
IET	Area	1.6×10^4	3.1×10^4	4.7×10^4	6.2×10^4	7.8×10^4	9.4×10^4	1.1×10^5	1.2×10^5	1.4×10^5	1.6×10^5	1.7×10^5
	R^2	0.76	0.83	0.77	0.74	0.77	0.77	0.75	0.77	0.75	0.78	0.76
	Adj R^2	0.4	0.57	0.43	0.36	0.44	0.43	0.39	0.44	0.37	0.44	0.4
	SSE	6.26	4.47	5.94	6.69	5.82	5.94	6.34	5.76	6.49	5.72	6.16
	RMS	0.4	0.33	0.39	0.41	0.38	0.38	0.4	0.38	0.4	0.38	0.39
IES	Area	1.8×10^4	3.5×10^4	5.3×10^4	7.1×10^4	8.9×10^4	1.1×10^5	1.2×10^5	1.4×10^5	1.6×10^5	1.8×10^5	2.0×10^5
	R^2	1	1	1	1	1	1	1	1	1	1	1
	Adj R^2	0.99	0.99	0.99	0.99	0.99	0.99	0.99	0.99	1	0.99	0.99
	SSE	0.003	0.002	0.003	0.003	0.003	0.003	0.002	0.001	0.001	0.001	0.001
	RMS	0.009	0.007	0.008	0.008	0.009	0.008	0.007	0.006	0.005	0.006	0.006
IFCR	Area	2.8×10^4	5.6×10^4	8.4×10^4	1.1×10^5	1.4×10^5	1.7×10^5	1.9×10^5	2.2×10^5	2.5×10^5	2.7×10^5	3.0×10^5
	R^2	0.78	0.78	0.72	0.74	0.8	0.75	0.81	0.74	0.76	0.68	0.67
	Adj R^2	0.46	0.45	0.31	0.35	0.5	0.37	0.53	0.36	0.4	0.22	0.17
	SSE	4913.31	4737.99	5613.29	4967.08	3726.95	4633.05	3429.65	4679.59	4418.54	5766.31	6140.52
	RMS	11.19	10.99	11.97	11.26	9.75	10.85	9.35	10.92	10.62	12.13	12.52
ETC	Area	5.4×10^1	1.1×10^2	1.6×10^2	2.2×10^2	2.8×10^2	3.3×10^2	3.9×10^2	4.5×10^2	5.0×10^2	5.6×10^2	6.2×10^2
	R^2	0.788	0.781	0.724	0.739	0.802	0.751	0.814	0.745	0.759	0.689	0.671
	Adj R^2	0.469	0.452	0.309	0.348	0.504	0.377	0.535	0.362	0.398	0.222	0.176
	SSE	0.02	0.02	0.025	0.023	0.017	0.022	0.016	0.023	0.022	0.03	0.033
	RMS	0.022	0.023	0.025	0.024	0.021	0.023	0.02	0.024	0.024	0.028	0.029
ESC	Area	1.1×10^2	2.2×10^2	3.3×10^2	4.5×10^2	5.6×10^2	6.7×10^2	7.8×10^2	9.0×10^2	1.0×10^3	1.1×10^3	1.2×10^3
	R^2	0.822	0.869	0.824	0.801	0.826	0.817	0.799	0.812	0.783	0.807	0.792
	Adj R^2	0.554	0.672	0.56	0.503	0.565	0.542	0.497	0.529	0.457	0.517	0.479
	SSE	0	0	0	0	0	0	0	0	0	0	0
	RMS	0.003	0.002	0.003	0.003	0.003	0.003	0.003	0.003	0.003	0.003	0.003
ED	Area	1.9×10^4	3.7×10^4	5.5×10^4	7.2×10^4	9.0×10^4	1.1×10^5	1.2×10^5	1.4×10^5	1.6×10^5	1.7×10^5	1.9×10^5
	R^2	0.787	0.783	0.725	0.743	0.802	0.751	0.815	0.747	0.761	0.689	0.671
	Adj R^2	0.467	0.457	0.311	0.358	0.504	0.378	0.538	0.368	0.402	0.222	0.176
	SSE	4896.87	4721.42	5595.32	4950.75	3716.68	4620.39	3421.22	4665.06	4404.92	5749.95	6123.26
	RMS	11.18	10.978	11.951	11.241	9.74	10.86	9.345	10.912	10.604	12.115	12.502

Table 6. Eligible ACC speeds—EOC criteria (100 time steps = 1 s).

Area	R^2	Adj R^2	SSE	RMS	Area	R^2	Adj R^2	SSE	RMS	Area	R^2	Adj R^2	SSE	RMS
		IE					**IES**					**IFCR**		
75	69	69	70	70	75	68	68	75	75	65	66	66	75	75
74	70	70	69	69	74	71	71	71	71	66	69	69	66	66
73	65	65	71	71	73	70	70	68	68	67	75	75	69	69
72	68	68	72	72	72	69	69	70	70	68	65	65	65	65
71	71	71	68	68	71	67	67	72	72	69	70	70	70	70
70	73	73	73	73	70	72	72	74	74	70	67	67	72	72
		ETC					**ESC**					**ED**		
75	66	66	66	66	75	69	69	70	70	65	66	66	75	75
74	69	69	65	65	74	70	70	69	69	66	69	69	66	66
73	75	75	69	69	73	68	68	71	71	67	75	75	69	69
72	65	65	75	75	72	65	65	72	72	68	65	65	70	70
71	70	70	70	70	71	71	71	73	73	69	70	70	65	65
70	67	67	67	67	70	66	66	68	68	70	67	67	72	72

Table 7. ACC speeds—10 s, SL = 75 MPH.

T_1	T_2	T_3	T_4	T_5	T_6	T_7	T_8	T_9	T_{10}
69	68	66	75	74	67	67	75	67	75
71	70	65	68	72	71	72	66	75	71
68	71	67	65	65	74	73	68	73	65

5. Experimental Results

A series of experiments are designed, analysed and evaluated on a real-time dataset to evaluate the performance of the proposed framework.

5.1. Dataset Retrieval

We conducted this research using three test vehicles, a 2019 Cadillac XT6, a 2020 Cadillac CT5, and a 2021 Cadillac CT4, obtained from GMC. A two-step procedure was employed to retrieve the data from the vehicle CAN bus (Li et al., 2008) [33]. We connected the hardware neoVI to the vehicle and retrieved the data retrieval using the software Vehicle Spy. This tool records data in real-time (Gallardo, 2018) and allows the user to selectively retrieve the signal data required for analysis [34]. We performed the real-time test procedure by activating the ACC feature, and time-step snippets of data were collected for each vehicle at a frequency of 10 Hz, i.e., 100 data points are recorded for 1s assuming a no-slip (Eathakota et al., 2008) [28,29].

The test cases are developed by driving the vehicles on selected road segments covering all the arterial, state ways, and freeways scenarios. Shown in Figure 4 are the paths traversed by the Cadillac test vehicles. The properties of the six datasets used for this analysis, including the input and output parameters of the DL model, are shown in Tables 8–10. Please find the details of the predictive model in the following sections.

5.2. Prediction of EOP

The properties of the NARX model and the test cases used for training are shown in Table 1. We developed individual training networks with default properties using the DL toolbox of MATLAB for the three vehicles' test data and the predicted EOP's, as shown in the Supplementary Materials, Figures S1–S6. Each figure consists of three parts: IET (left), IES (middle), and IFCR (right). Furthermore, each plot compares the measured data (blue) with the predicted values (orange). We validated the performance of the NARX DL model prediction using traditional statistical techniques (RMSE, FOD, SNR) to compare the actual and predicted values of EOP, as reported in Table 11. We conclude that IES follows a smooth curve, whereas IFCR and IET oscillate.

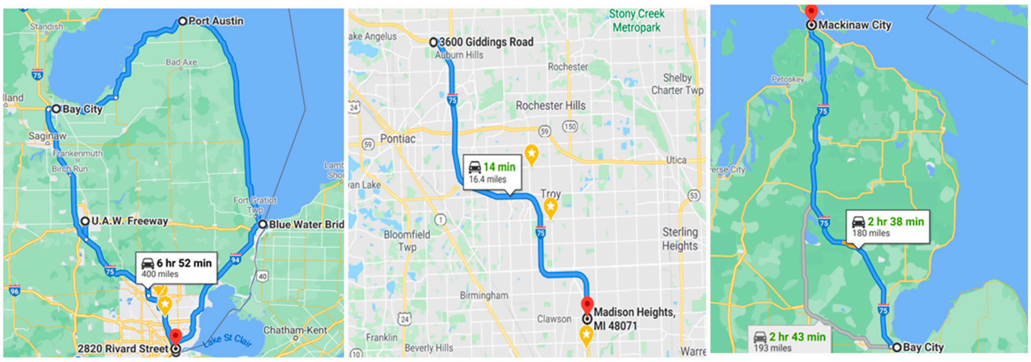

Cadillac CT5, ACC Speed = [25 65] MPH   Cadillac XT6, ACC Speed = [65 75] MPH   Cadillac CT4, ACC Speed = [75 85] MPH

Figure 4. Path traversed—GMC test vehicles (Google Maps).

Table 8. Data Set 1: 2020 Cadillac CT5—arterial roads.

Parameters	ACC Speed [25 35] MPH			ACC Speed [35 45] MPH		
Inputs	**Mean**	**StdDev**	**Variance**	**Mean**	**StdDev**	**Variance**
Absolute time (s)	2468.020	1655.047	0.671	4584.239	2453.828	0.535
Odometer (km)	11,721.440	41.765	0.004	11,596.730	56.886	0.005
Speed (MPH)	30.831	2.859	0.093	40.634	2.768	0.068
Acceleration ($m{\cdot}s^{-2}$)	1.090	0.652	0.598	0.808	0.449	0.556
LOT ($m{\cdot}s^{-2}$)	0.933	0.633	0.678	0.670	0.411	0.614
LAT ($m{\cdot}s^{-2}$)	0.318	0.637	2.002	0.362	0.335	0.924
YAR (deg/s)	0.098	2.633	26.944	0.179	1.056	5.914
EAT (°F)	12.964	0.688	0.053	14.727	1.742	0.118
CAT (°F)	66.141	0.348	0.005	68.895	1.069	0.016
TPFL (kPa)	225.908	2.915	0.013	226.990	3.243	0.014
TPRL (kPa)	235.773	4.640	0.020	239.900	4.259	0.018
TPFR (kPa)	235.115	4.834	0.021	235.575	3.706	0.016
TPRR (kPa)	234.132	5.742	0.025	237.544	4.270	0.018
Outputs	**Mean**	**StdDev**	**Variance**	**Mean**	**StdDev**	**Variance**
IET (Nm)	173.081	45.424	0.262	186.309	30.686	0.165
IES (rad/s)	219.483	82.421	0.376	222.809	73.464	0.330
IFCR (1×10^{-8} m^3s^{-1})	380.687	204.214	0.536	378.523	139.192	0.368

5.3. Estimation of Optimal ACCSSP

The developed DL model and the steps defined in Section 4 are used to estimate the optimal ACCSSP for each test case. An example, for the test case of the vehicle 2019 Cadillac XT6, is selected with the AVS = [65 75] MPH, and the corresponding results are shown in Tables 4–6. The IAS (S_0) is varied in the range [65 75] MPH for the ACC Matrix (Table 7), and Step 4 is applied to the EVS, which results in eight ACCSSP's shown in Figure 5. Thus for S_0 = 70 MPH, the predicted ACCSSP is the row vector ((71, 71, 71, 71, 72, 72, 73, 73, 74, 74) MPH) as shown in Figure S8. We adopted a similar procedure for multiple data sets and plotted the predicted ACCSSP's are presented in the Supplementary Materials, Figures S7–S12. Please find the performance of EOC parameters for the predicted ACCSSP's in Section B: Table 12.

Table 9. Data Set 2: 2020 Cadillac CT5—state ways roads.

Parameters	**ACC Speed [45 55] MPH**			**ACC Speed [55 65] MPH**		
Inputs	**Mean**	**StdDev**	**Variance**	**Mean**	**StdDev**	**Variance**
Absolute time (s)	3701.490	1808.730	0.489	2933.845	1442.236	0.492
Odometer (km)	11,410.820	42.130	0.004	11,894.840	36.372	0.003
Speed (MPH)	51.354	2.605	0.051	60.707	2.821	0.046
Acceleration ($m{\cdot}s^{-2}$)	0.500	0.210	0.420	0.415	0.208	0.501
LOT ($m{\cdot}s^{-2}$)	0.336	0.208	0.619	0.257	0.214	0.835
LAT ($m{\cdot}s^{-2}$)	0.256	0.193	0.751	0.305	0.180	0.590
YAR (deg/s)	−0.190	0.534	−2.805	−0.030	0.473	−15.914
EAT (°F)	12.889	0.556	0.043	15.083	0.670	0.044
CAT (°F)	69.726	0.688	0.010	66.000	0.000	0.000
TPFL (kPa)	235.424	3.508	0.015	239.108	2.371	0.010
TPRL (kPa)	233.685	3.947	0.017	237.436	2.193	0.009
TPFR (kPa)	226.567	3.062	0.014	228.252	0.972	0.004
TPRR (kPa)	233.767	3.764	0.016	238.294	2.279	0.010
Outputs	**Mean**	**StdDev**	**Variance**	**Mean**	**StdDev**	**Variance**
IET (Nm)	234.943	25.244	0.107	254.370	27.752	0.109
IES (rad/s)	167.982	28.195	0.168	180.272	36.291	0.201
IFCR (1×10^{-8} m^3s^{-1})	374.715	82.660	0.221	441.351	109.691	0.249

Table 10. Data Set 3: 2019 Cadillac XT6, 2021 Cadillac CT4—freeways roads.

Parameters	**Cadillac XT6, ACC Speed [65 75] MPH**			**Cadillac CT4, ACC Speed [75 85] MPH**		
Inputs	**Mean**	**StdDev**	**Variance**	**Mean**	**StdDev**	**Variance**
Absolute time (s)	387.430	223.687	0.577	31.709	12.962	0.409
Odometer (km)	12,723.040	7.015	0.001	30,298.330	17.042	0.001
Speed (MPH)	70.121	1.149	0.016	77.905	1.501	0.019
Acceleration ($m{\cdot}s^{-2}$)	0.004	0.242	67.073	0.081	0.177	2.175
LOT ($m{\cdot}s^{-2}$)	−0.091	0.188	−2.079	0.108	0.189	1.748
LAT ($m{\cdot}s^{-2}$)	0.132	0.339	2.572	−0.149	0.307	−2.057
YAR (deg/s)	0.230	0.851	3.698	−0.256	0.694	−2.710
EAT (°F)	39.225	0.296	0.008	85.039	0.998	0.012
CAT (°F)	68.785	0.301	0.004	66.502	0.862	0.013
Pitch angle (deg)	−0.262	0.742	−2.836	−0.003	0.002	−0.771
TPFL (kPa)	241.238	2.428	0.010	227.807	0.289	0.001
TPRL (kPa)	235.890	0.655	0.003	249.502	0.290	0.001
TPFR (kPa)	243.691	1.069	0.004	228.316	0.409	0.002
TPRR (kPa)	235.224	1.582	0.007	249.503	0.287	0.001
Outputs	**Mean**	**StdDev**	**Variation**	**Mean**	**StdDev**	**Variance**
IET (Nm)	146.803	63.428	0.432	142.117	33.698	0.237
IES (rad/s)	183.081	7.105	0.039	205.343	17.341	0.084
IFCR (1×10^{-8} m^3s^{-1})	387.430	223.687	0.577	31.709	12.962	0.409

Table 11. NARX DL model performance—ACCSSP [30 80] MPH.

EOP	**IET**			**IES**			**IFCR**		
Metric	RMSE	FOD	SNR	RMSE	FOD	SNR	RMSE	FOD	SNR
30 MPH	2.761	1.911	35.003	2.367	1.541	35.417	12.911	8.717	25.499
40 MPH	0.750	0.418	45.362	0.845	0.484	37.442	14.122	9.477	24.418
50 MPH	1.263	0.811	45.566	1.400	0.932	43.413	18.966	13.289	25.495
60 MPH	0.590	0.417	51.103	0.521	0.348	51.414	21.740	15.241	25.582
70 MPH	0.322	0.186	53.762	0.228	0.169	58.007	8.335	5.877	30.369
80 MPH	0.576	0.618	46.651	0.064	0.027	70.160	9.917	6.879	27.586

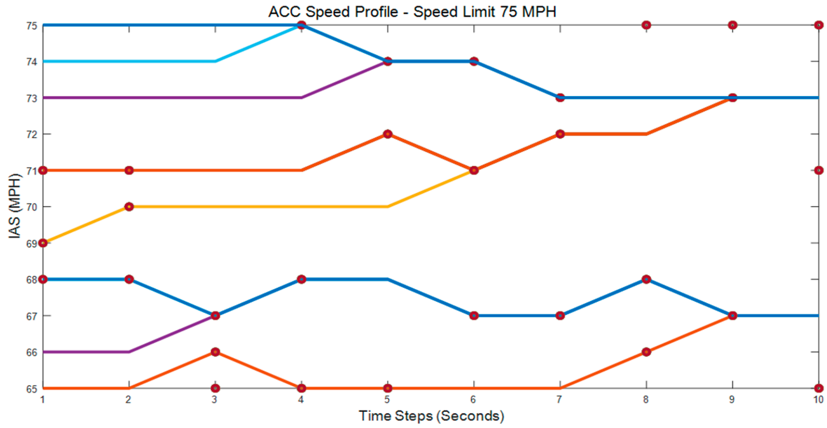

Figure 5. Predicted ACCSSP, IAS = [65 75] MPH, SL = 75 MPH.

Table 12. EOC criteria: engine parameters (predicted–constant) ACCSSP.

Section: A				**Section: B**						
Data	IAS = 70 MPH, SL = 75 MPH			Speed (MPH)		Test Cases				
Metric	ACCSSP (70 MPH)	ACCSSP (Predicted)	Conformance	SL	IAS	Distance	ED	IFCR	ETC	ESC
				35	30	0.22	−17.33	−21.19	0.25	−0.26
Distance	69,930.00	72,028.00	934.77	45	40	133.44	−64.11	−52.113	−0.27	0.50
ED	17,4570.83	17,4196.86	−373.96	55	50	712.22	−366.13	−323.27	0.51	1.20
ETC	572.12	573.34	1.22	65	60	−312.11	−510.75	−540.58	0.87	0.22
ESC	1154.63	1164.83	10.20	75	70	934.77	−373.96	−379.09	1.22	10.20
IFCR	27,4182.80	27,3803.70	−379.09	85	80	801.108	−1035.28	−1029.6	2.813	−2.022

6. Discussion

The plots of predicted EOP's for the three test vehicles Cadillac CT5, XT6, and CT4, are depicted in Figures S1–S6 The predictive model is validated by estimating the conformance between actual and predicted data's RMSE, FOD, and SNR (Table 11). The IET RMSE values were <2.76, whereas IES FOD was <1.54 for all the datasets. We recorded the IFCR on a scale of 1×10^{-8} m^3s^{-1}, and the IFCR SNR has an acceptable range of [24.41–30.36]. Additionally, we can visualise that the predicted curves have a smoother fit to the actual data, and thus efficacy of the DL model to predict EOP is validated.

In this work, we proposed the criteria for augmented EOC and an iterative methodology to predict ACCSSP's, resulting in optimal EOP. Hence, for each future second, the AVS is varied in a definite range [65 75] MPH for the 2019 Cadillac XT6, and the corresponding inputs for the future states are fed into the DL model to generate multiple EOPs. We applied EOC criteria to the EOPs, and the top three EVS are estimated as [69,71,68] MPH.

We adopted a similar procedure for ten seconds and predicted ACCSSP for IAS = 70 MPH, SL = 75 MPH, with a minimum of 71 MPH and a maximum of 73 MPH (Figure S8). The predicted and constant ACCSSP profile (70 MPH) with corresponding inputs (Section 4.1) were fed into the DL model to obtain two different EOP's vectors (Section 4.2) for future time steps (10 s). We applied the EOC criteria for the two EOPs whose values are in Section A: Table 12 and thus predicted ACCSSP resulted in 934.77 m of the additional distance traversed and a reduced ED of 373.968. Additionally, the constant ACCSSP = 70 MPH consumed 379.095 1×10^{-8} m^3 more fuel in 10 s compared with the predicted ACCSSP.

The plots of engine performance parameters are shown in Figure 6, and the area under the curve has higher magnitudes by 1.2 (ETC) and 10.2 (ESC) for the predicted ACCSSP. Please find the smoothness measure for the conformance of the two EOP's in Table 13, and R^2/Adjusted R^2 have similar values (conformance~ 0), whereas RMSE/SSE have lower values for predicted ACCSSP for most cases. Section B: Table 12 depicts the performance of EOC parameters for all the test cases, and it is easy to see that in most cases, the predicted ACCSSP has reduced ED and IFCR. Hence the proposed approach in this article is novel and better suits enhancing EOC and lowering the trip time.

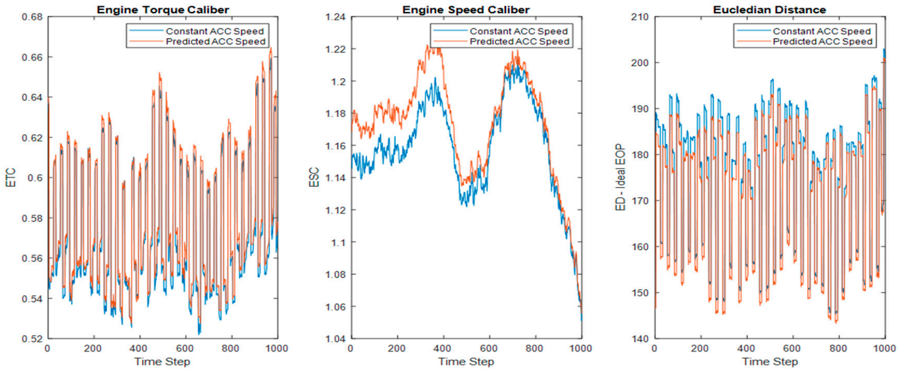

Figure 6. EOC Parameters—(ETC, ESC, ED); IAS = 70 MPH, SL = 75 MPH, 2019 Cadillac XT6.

Table 13. EOC criteria: smoothness performance—(predicted–constant) ACCSSP.

EOP		IET				IES				IFCR			
SL	IAS	R^2	Adj R^2	SSE	RMS	R^2	Adj R^2	SSE	RMS	R^2	Adj R^2	SSE	RMS
35	30	0.0	0.0	−9.415	−0.007	0.0	0.000	0.564	0.000	0.000	0.0	−103.786	−0.023
45	40	0.0	0.0	0.326	0.001	0.0	0.000	2.582	0.013	0.000	0.0	−23.251	−0.005
55	50	0.0	0.0	3.069	0.007	0.0	0.001	−38.090	−0.033	0.000	0.0	−570.595	−0.083
65	60	0.0	0.0	1.307	0.005	0.0	0.000	0.431	0.002	0.000	0.0	33.212	0.004
75	70	0.0	0.0	0.368	0.004	0.064	0.160	−2.607	−0.024	0.000	0.0	136.612	0.044
85	80	0.0	0.0	−0.312	−0.001	−0.002	−0.005	0.142	0.007	0.001	0.002	−243.889	−0.068

7. Conclusions and Future Work

In this manuscript, we developed a novel method to predict the ACCSSP, which optimises engine performance. We considered the vector EOP and used NARX DL modelling techniques to predict the EOP by mapping the VLV. We defined EOC criteria using the elements of EOP, which reflect enhanced engine operating conditions. In this methodology, a new approach of inputting the range of allowable ACC speeds is proposed and, therefore, a unique ACCSSP for the future time-steps was generated in the defined range by utilising iterative methods and satisfying the EOC criteria. The predicted and constant ACCSSP are fed into the DL model, and the engine performance parameters are estimated based on the predicted EOP. The results depict that for predicted ACCSSP, the parameters (ETC, ESC, IET, IES), and (IFCR, ED) have higher and lower values. Additionally, the predicted ACCSSP generated smoother profiles for the engine parameters when plotted in the time domain.

The researchers have not investigated the proposed technique of predicting ACCSSP, and this new approach could also trigger a new capability in ACC controllers to deviate from the user command of unique set speed and produce enhanced vehicle performance. The computational results obtained were satisfactory, and thus, we observed augmented EOC for the predicted ACCSSP.

We did not include many critical points, including traffic congestion, in the model. Future work would involve developing the model by including all the affecting parameters and performing extensive validation using multiple vehicle lines at various locations and periods. Additionally, this research could be extended to electric vehicles by defining new criteria of battery and motor operating conditions.

Supplementary Materials: The following are available online at https://www.mdpi.com/article/10.3390/vehicles3040044/s1, Figure S1: Prediction of EOP-ACCSSP = 30 MPH, 2020 Cadillac CT5;

Figure S2: Prediction of EOP-ACCSSP = 40 MPH, 2020 Cadillac CT5; Figure S3: Prediction of EOP-ACCSSP = 50 MPH, 2020 Cadillac CT5; Figure S4: Prediction of EOP-ACCSSP = 60 MPH, 2020 Cadillac CT5; Figure S5: Prediction of EOP-ACCSSP = 70 MPH, 2019 Cadillac XT6; Figure S6: Prediction of EOP-ACCSSP = 80 MPH, 2021 Cadillac CT4; Figure S7: Prediction of ACCSSP-IAS = 80 MPH, SL = 85 MPH; Figure S8: Prediction of ACCSSP-IAS = 70 MPH, SL = 75 MPH; Figure S9: Prediction of ACCSSP-IAS = 60 MPH, SL = 65 MPH; Figure S10: Prediction of ACCSSP-IAS = 50 MPH, SL = 55 MPH; Figure S11: Prediction of ACCSSP-IAS = 40 MPH, SL = 45 MPH; Figure S12: Prediction of ACCSSP-IAS = 30 MPH, SL = 35 MPH.

Author Contributions: The first author (S.K.) came up with the idea, developed the concept, and performed the analysis. The second author (H.M.) is the principal investigator for this project. All authors have read and agreed to the published version of the manuscript.

Funding: The project "Predictive model of ACCSSP" was performed under the University of Michigan and GMC research collaboration, funded by William J. Clifford (Director) of the Systems Engineering department at GMC.

Institutional Review Board Statement: Not applicable.

Informed Consent Statement: Not applicable.

Data Availability Statement: The data used in this work are proprietary to GMC and cannot be made publicly available. However, the modelling algorithm is available on request.

Acknowledgments: The authors would like to thank Iqbal Surti, Systems Engineer at GMC, for his assistance in real-time testing. The technical analysis was performed using the tools provided by GMC (Vehicle Spy and neoVI) and the University of Michigan (MATLAB).

Conflicts of Interest: The authors of this manuscript declare that there is no conflict of interest regarding the publication of this article.

Abbreviations

ACC	Adaptive cruise control
ACCSSP	Adaptive cruise control set speed profile (MPH)
Area	Area under the curve
AVS	Allowable vehicle speeds
CAN	Controller area network
CAT	Cabin air temperature (°F)
DL	Deep Learning
DBV	Driver behaviour vector
EAT	External air temperature (°F)
ED	Euclidean distance—Ideal EOP and Predicted EOP
EOC	Engine operating conditions
EOP	Engine operating point
ESC	Engine speed caliber
EVS	Eligible vehicle speeds
ETC	Engine torque caliber
FOD	First order derivative
IAS	Initial ACC speed (MPH)
IEM	Instantaneous engine map
IES	Instantaneous engine speed (rad/s)
IET	Instantaneous engine torque (Nm)
IFCR	Instantaneous fuel consumption rate (1×10^{-8} m^3s^{-2})
ISB	Ideal steering behaviour
LAT	Lateral acceleration ($m\cdot s^{-2}$)
LOT	Longitudinal acceleration ($m\cdot s^{-2}$)
LSTM	Long short-term memory
GMC	General motors corporation
MPH	Miles per hour

MY	Model year
NARX	Autoregressive network with exogenous inputs
OEM	Original equipment manufacturer
RMSE	Root mean square error
RRC	Radius of road curvature (m)
SL	Speed limit (MPH)
SNR	Signal to noise ratio
SSEStdDev	Sum of squared errorsStandard deviation
TP	Tire pressure (kPa)
TPFL	Tire pressure front left (kPa)
TPFR	Tire pressure front right (kPa)
TPRL	Tire pressure rear left (kPa)
TPRR	Tire pressure rear right (kPa)
VLV	Vehicle level vectors
YAR	Yaw rate (rad/s)

Nomenclature

A_c	Area of vehicle cross-section (m^2)
C_d	Aerodynamic drag coefficient
°F	Fahrenheit
g	Gravity
Hz	Hertz
kPa	Kilopascals
Kg	Kilogram
Km	Kilometres
kWh	Kilowatt-hour
$L_{a(k)}$	Lateral acceleration at time step k ($m{\cdot}s^{-2}$)
$L_{o(k)}$	Longitudinal acceleration at time step k ($m{\cdot}s^{-2}$)
M_c	Mass of the vehicle. (Kg)
M_L	Mass of the additional load (Kg)
MPH	Miles per hour
m	Meters
m^2	Meter square (measure of area)
m^3s^{-1}	Meter cube per second (volume rate flow)
$m.s^{-2}$	Meters per second square
ms	Milli seconds
Nm	Newton meter
μ_r	Rolling coefficient
rad	Radians
rad/s	Radians per second
RRC_k	Radius of road curvature at time step k (m)
RPM	Rotations per minute
ρ	Density of air ($kg.m^{-3}$)
s	Seconds
T_k	Timestep
dT	Incremental time step (~10 ms)
$\theta_{g(k)}$	Gradient of the terrain at time step k (rad)
$Y_{a(k)}$	Yaw rate at time step k (rad/s)
m^3s^{-1}	Meter cube per second (Volume rate flow)

References

1. Townsend, J.D.; Calantone, R.J. Evolution and Transformation of Innovation in the Global Automotive Industry. *J. Prod. Innov. Manag.* **2014**, *31*, 4–7. [CrossRef]
2. Katzenbach, A. Automotive. In *Concurrent Engineering in the 21st Century*; Springer: Cham, Switzerland, 2015; pp. 607–638.
3. Labuhn, P.I.; Chundrlik, W.J., Jr. Adaptive Cruise Control. U.S. Patent 5,454,442, 3 October 1995.

4. Marsden, G.; McDonald, M.; Brackstone, M. Towards an understanding of adaptive cruise control. *Transp. Res. Part C Emerg. Technol.* **2001**, *9*, 33–51. [CrossRef]
5. Mahdinia, I.; Arvin, R.; Khattak, A.J.; Ghiasi, A. Safety, Energy, and Emissions Impacts of Adaptive Cruise Control and Cooperative Adaptive Cruise Control. *Transp. Res. Rec. J. Transp. Res. Board* **2020**, *2674*, 253–267. [CrossRef]
6. Stanton, N.A.; Young, M.S. Driver behaviour with adaptive cruise control. *Ergonomics* **2005**, *48*, 1294–1313. [CrossRef]
7. Hoedemaeker, M.; Brookhuis, K. Behavioural adaptation to driving with an adaptive cruise control (ACC). *Transp. Res. Part F Traffic Psychol. Behav.* **1998**, *1*, 95–106. [CrossRef]
8. Kesting, A.; Treiber, M.; Schönhof, M.; Kranke, F.; Helbing, D. Jam-avoiding adaptive cruise control (ACC) and its impact on traffic dynamics. In *Traffic and Granular Flow'05*; Springer: Berlin, Heidelberg, 2007; pp. 633–643.
9. Rudin-Brown, C.M.; Parker, H.A. Behavioural adaptation to adaptive cruise control (ACC): Implications for preventive strategies. *Transp. Res. Part F Traffic Psychol. Behav.* **2004**, *7*, 59–76. [CrossRef]
10. Moon, S.; Yi, K. Human driving data-based design of a vehicle adaptive cruise control algorithm. *Veh. Syst. Dyn.* **2008**, *46*, 661–690. [CrossRef]
11. Rosenfeld, A.; Bareket, Z.; Goldman, C.V.; Leblanc, D.J.; Tsimhoni, O. Learning Drivers' Behavior to Improve Adaptive Cruise Control. *J. Intell. Transp. Syst.* **2015**, *19*, 18–31. [CrossRef]
12. Milanes, V.; Shladover, S.E.; Spring, J.; Nowakowski, C.; Kawazoe, H.; Nakamura, M. Cooperative Adaptive Cruise Control in Real Traffic Situations. *IEEE Trans. Intell. Transp. Syst.* **2013**, *15*, 296–305. [CrossRef]
13. Milanés, V.; Shladover, S.E. Modeling cooperative and autonomous adaptive cruise control dynamic responses using experimental data. *Transp. Res. Part C Emerg. Technol.* **2014**, *48*, 285–300. [CrossRef]
14. Kesting, A.; Treiber, M.; Schönhof, M.; Helbing, D. Adaptive cruise control design for active congestion avoidance. *Transp. Res. Part C Emerg. Technol.* **2008**, *16*, 668–683. [CrossRef]
15. Ploeg, J.; Serrarens, A.F.A.; Heijenk, G.J. Connect & Drive: Design and evaluation of cooperative adaptive cruise control for congestion reduction. *J. Mod. Transp.* **2011**, *19*, 207–213. [CrossRef]
16. Lin, D.-Y.; Hou, B.-J.; Lan, C.-C. A balancing cam mechanism for minimizing the torque fluctuation of engine camshafts. *Mech. Mach. Theory* **2017**, *108*, 160–175. [CrossRef]
17. Lu, C.; Dong, J.; Hu, L. Energy-Efficient Adaptive Cruise Control for Electric Connected and Autonomous Vehicles. *IEEE Intell. Transp. Syst. Mag.* **2019**, *11*, 42–55. [CrossRef]
18. Vedam, N. Terrain-Adaptive Cruise Control: A Human-Like Approach. Ph.D. Thesis, Texan A&M University, Collage Station, TX, USA, 2015.
19. Kolmanovsky, I.V.; Filev, D.P. Terrain and Traffic Optimized Vehicle Speed Control. *IFAC Proc. Vol.* **2010**, *43*, 378–383. [CrossRef]
20. Gaspar, P.; Németh, B. Design of adaptive cruise control for road vehicles using topographic and traffic information. *IFAC Proc. Vol.* **2014**, *47*, 4184–4189. [CrossRef]
21. Németh, B.; Gáspár, P. Road inclinations in the design of LPV-based adaptive cruise control. *IFAC Proc. Vol.* **2011**, *44*, 2202–2207. [CrossRef]
22. Németh, B.; Gaspar, P. Design of vehicle cruise control using road inclinations. *Int. J. Veh. Auton. Syst.* **2013**, *11*, 313. [CrossRef]
23. Ma, J.; Hu, J.; Leslie, E.; Zhou, F.; Huang, P.; Bared, J. An eco-drive experiment on rolling terrains for fuel consumption optimization with connected automated vehicles. *Transp. Res. Part C Emerg. Technol.* **2019**, *100*, 125–141. [CrossRef]
24. Kolachalama, S.; Lakshmanan, S. *Using Deep Learning to Predict the Engine Operating Point in Real-Time*; SAE Technical Paper; General Motors LLC: Detroit, MI, USA, 2021.
25. Diaconescu, E. The use of NARX neural networks to predict chaotic time series. *Wseas Trans. Comput. Res.* **2008**, *3*, 182–191.
26. Kolachalama, S.; Hay, C.L.; Mushtarin, T.; Todd, N.; Heitman, J.; Hermiz, S. *An Algorithm to Estimate Steering Behavior Using Vehicle Radius of Curvature*; Research Disclosure, Questel Ireland Ltd.: Paris, France, 2018; p. 647068.
27. Kolachalama, S.; Kuppa, K.; Mattam, D.; Shukla, M. Thermal Analysis of Radiator Core in Heavy Duty Automobile. In Proceedings of the Heat Transfer Summer Conference, Jacksonville, FL, USA, 10–14 August 2008; Volume 48487, pp. 123–127.
28. Eathakota, V.P.; Kolachalama, S.; Krishna, K.M.; Sanan, S. Optimal posture control for force actuator based articulated suspension vehicle for rough terrain mobility. In *Advances in Mobile Robotics*; World Scientific: Coimbra, Portugal, 2008; pp. 760–767.
29. Eathakota, V.; Singh, A.K.; Kolachalama, S.; Madhava Krishna, K. Determination of Optimally Stable Posture for Force Actuator Based Articulated Suspension for Rough Terrain Mobility. In *Trends in Intelligent Robotics. FIRA 2010*; Communications in Computer and Information Science; Springer: Berlin/Heidelberg, Germany, 2010; Volume 103.
30. Tanaka, H.; Tokushima, T.; Higashi, H.; Hamada, S. Means for Suppressing Engine Output Torque Fluctuations. U.S. Patent 4,699,097, 13 October 1987.
31. Li, S.E.; Guo, Q.; Xu, S.; Duan, J.; Li, S.; Li, C.; Su, K. Performance Enhanced Predictive Control for Adaptive Cruise Control System Considering Road Elevation Information. *IEEE Trans. Intell. Veh.* **2017**, *2*, 150–160. [CrossRef]
32. La Valle, S.M. Motion planning. *IEEE Robot. Autom. Mag.* **2011**, *18*, 108–118. [CrossRef]
33. Li, R.; Liu, C.; Luo, F. A design for automotive CAN bus monitoring system. In Proceedings of the 2008 IEEE Vehicle Power and Propulsion Conference, Harbin, China, 3–5 September 2008; pp. 1–5.
34. Gallardo, F.B. Extraction and Analysis of Car Driving Data via Obd-II. Ph.D. Thesis, Universidad Miguel Hernández de Elche, Alicante, Spain, 2018.